Decoupling Diameter and Pitch in Silicon Nanowire Arrays Made by Metal-Assisted Chemical Etching

*Junghoon Yeom, Daniel Ratchford, Christopher R. Field, Todd H. Brintlinger, and Pehr E. Pehrsson**

The fabrication of well-separated, narrow, and relatively smooth silicon nanowires with good periodicity is demonstrated, using non-close-packed arrays of nanospheres with precisely controlled diameters, pitch, and roughness. Controlled reactive ion etching in an inductively coupled plasma reduces the self-assembled nanospheres to approximately a tenth of their original diameter, while retaining their surface smoothness and periodic placement. A titanium adhesion layer between the silicon substrate and gold film allows much thinner catalyst layers to be continuous, facilitating the film liftoff and formation of the perforated pattern without influencing catalyzed etching of silicon. Using these methods, a periodic array of silicon nanowires with a large pitch and small diameter (e.g., a 490 nm pitch and 55 nm diameter) is created, a combination not typically found in the open literature. This approach extends the types and quality of silicon nanostructures that can be fabricated using the combined nanosphere lithography and metal-assisted chemical etching techniques.

1. Introduction

Silicon nanowires (SiNWs) display exceptional physical and chemical properties[1] and have been explored as potential building blocks for numerous functional devices, including circuit elements,[2] solar cells,[3] and chemical/biological sensors.[4] Vapor-liquid-solid growth is the most commonly used bottom-up method to produce a large number of these SiNWs,[5] but the high temperature required for synthesis, the incorporation of metal impurities, the difficulties in controlling NW diameter and doping levels, and lack of large-scale NW placement technology hinder widespread acceptance in industry.[6] Alternatively, arrays of vertically aligned silicon nanowires (VA-SiNWs) that are etched from a bulk Si substrate have drawn increasing attention, since the dopant type and concentration and crystal orientation of SiNWs are the same as the substrate and thus can be precisely controlled, providing opportunities for vertical field-effect transistors[7] and optoelectronic devices.[8] Unique optical properties that are substantially different from those of bulk Si have been recently reported for VA-SiNW arrays, whose diameters and pitches are smaller than the wavelength of light.[9] Because accurate control of the diameters and pitches of VA-SiNW arrays is critical to these electrical and/or optical applications, top-down fabrication technologies such as electron beam lithography (or photolithography) and reactive ion etching (RIE) are frequently employed to produce these ordered arrays but are either too slow to create large-area arrays or too expensive for anything but research environments.

We create VA-SiNW arrays using a metal-assisted chemical etching (MACE) process combined with bottom-up nanosphere lithography (NSL). This combined technique is simple, low-cost, and produces large-area, ordered SiNW arrays with the ability to tune the wire density and dimensions.[10] In the MACE process, silicon underneath a thin layer of noble metal (e.g., Ag, Au, Pt, etc.) is preferentially oxidized and anisotropically etched in aqueous solutions containing hydrogen fluoride (HF) and an oxidant (e.g., H_2O_2 or O_2 present in H_2O), leaving bare silicon regions unetched.[11] The noble metal acts as a microscopic cathode on which reduction of the oxidant generates holes.[12] These holes diffuse through the metal catalyst and are subsequently injected into the Si that is in contact with the noble metal, causing the Si to be oxidized and dissolved by HF.[13] This spontaneous bipolar electrochemical reaction produces an electric field driving the directional movement of the metal/Si interface and anisotropic dissolution of Si.[14]

Several routes have been used to generate VA-SiNW arrays using MACE.[15] One of the most heavily used approaches is to etch Si substrates with a catalyst mesh composed of random networks of metallic nanoparticles deposited by galvanic displacement from a mixture solution of HF and metal salt (e.g.,

Dr. J. Yeom, Dr. D. Ratchford
National Research Council Research Associateship Program
US Naval Research Laboratory
Washington, DC 20375, USA
Dr. C. R. Field, Dr. P. E. Pehrsson
Chemistry Division
US Naval Research Laboratory
Washington, DC 20375, USA
E-mail: pehr.pehrsson@nrl.navy.mil
Dr. T. H. Brintlinger
Material Science & Technology Division
US Naval Research Laboratory
Washington, DC 20375, USA

DOI: 10.1002/adfm.201301094

$AgNO_3$)[16] or by physical vapor deposition.[15] The resulting NW arrays are very dense but lack spatial ordering, and have a broad diameter distribution, restricting their use to applications where the exact location and morphology of NWs is less important.[17] Examples include antireflection coatings,[18] superhydrophobic/superhydrophilic surfaces,[19] photocatalysts,[20] Li-ion batteries,[21] and chemical/biological sensors.[22] On the other hand, well-ordered arrays of VA-SiNWs with consistent pitch, diameter, and surface morphology are necessary for applications whose device performance is highly sensitive to the geometrical parameters, for example, photovoltaics,[23] photonic crystal devices,[24] and electronic devices.[25] These ordered SiNW arrays typically begin with a periodic metal mesh atop the silicon surface. This periodic metal mesh can be patterned using top-down patterning techniques (e.g., electron beam lithography[12,13] and laser interference lithography)[26] or by masks prepared using bottom-up template-based approaches such as nanosphere lithography (NSL),[10a,27] block copolymer lithography,[28] and porous anodic alumina membrane.[29] Among these bottom-up approaches, NSL is the most popular method because it can be modified to produce a wide range of NW diameters and densities.[10a] NSL employs an array of hexagonally close-packed polystyrene (PS) colloidal spheres as a template for creating a nanomesh of the metal catalyst layer. The diameter of the spheres is typically first reduced to separate them, ultimately leading to hexagonal non-close-packed arrays of SiNWs.

Accurate control over the nanosphere (NS) array is critical since the diameter of the resulting SiNWs reflects the sphere diameter and spacing (i.e., array density). While the NW array pitch is determined by the initial NS diameter, the diameter of the resulting NWs can be adjusted by reducing the NS diameter. Various techniques are used to generate non-close-packed arrays of the colloidal spheres: gel trapping,[30] templating by spin-coating,[31] soft lithographic transfer,[32] electron irradiation,[33] and reactive ion etching (RIE).[34] Among these, RIE is the most suitable for parallel processing and compatibility with other device fabrication steps. However, plasma etching of NSs almost inevitably roughens the sphere surfaces and distorts their spherical shape.[35] As a result, the NWs made from these spheres have rough sidewalls and non-circular cross-sections, making it difficult to independently control the NW diameter and the array pitch. Etching using inductively coupled plasma (ICP)-RIE at cryogenic temperatures have been shown to result in smooth, isotropic size reduction of the PS NSs,[36] but to the best of our knowledge, large-scale size reduction (>70%) has not been demonstrated.

In this paper, we present the fabrication of an ordered, sparse SiNW array using the ultra-large-reduction of NSs to form a sparsely perforated metal film as a catalyst for MACE. While the top-down fabrication methods have been routinely employed to create sparse, ordered NWs,[37] an inexpensive, scalable bottom-up method for such NW arrays has been rarely reported. Our method is shown to reduce NS diameter by ≈90% while maintaining the surface smoothness and hexagonal array placement, enabling decoupling of diameter and pitch in SiNW arrays and further design flexibility. Once NSs are reduced to a fifth of their original diameter, metal lift-off and MACE steps pose additional challenges. For greatly reduced NSs, the NS size is comparable to the metal film thickness. As a result, the metal film encapsulates the NS, which inhibits NS liftoff. We show that angle-resolved deposition of the metal film or the use of an adhesion layer with a reduced metal film thickness allows an improved NS removal. Titanium is found to be an effective adhesion layer between the Au catalyst and Si without delaying Si etching. Another challenge is that MACE with a sparsely perforated Au film causes the tips of resulting NWs to be undesirably tapered and porous. Through a careful study of the Si etch rate as a function of the catalyst coverage, we optimize the etching parameters to minimize the tapering and porosity in SiNWs. A highly regular array of SiNWs with 490 nm pitch and 55 nm diameters was demonstrated. The large separation between SiNWs in a sparse array provides an opportunity to engineer various core-shell or other nanostructures around SiNWs. These large-area, ordered, sparse SiNWs created using NSL and MACE have numerous applications in optical applications such as photonic crystals[24,38] and biological applications, such as cell growth platforms.[39]

2. Results and Discussion

Figure 1a shows the three key fabrication steps to generate an array of SiNWs using NSL and MACE. Each of these key steps, depicted in the SEM images in Figure 1b–e, poses critical challenges to the creation of a sparse NW array. Assuming that a two-dimensional hexagonal close-packed array of PS NSs can be reproducibly formed on a substrate, the first critical challenge is large-scale reduction of the NS size. The pitch of the NW array is determined by the interparticle distance of the close-packed array, which is fixed by the original size of the NSs. Therefore, large-scale reduction of the NS diameter is necessary to make a well-separated NW array. RIE has been the most popular method to etch the NSs and form a two-dimensional hexagonal non-close-packed array because of its rapid and scalable nature.[10a] However, once the diameters of the NSs are reduced by more than approximately half, their spherical morphology, surface smoothness, and placement in the hexagonal NS array degrade. Figure 1b shows the roughened PS NSs during etching in a conventional parallel plate RIE. When the 490 nm NSs were reduced to below 250 nm, undesirable roughness emerged on the NS surfaces, distorting their spherical morphology. Since the morphology of the reduced NSs translates directly to the NW cross-section, it is important to precisely control their shape as well as roughness during etching. Conserving the hexagonal symmetry of close-packed arrays is also problematic since some of the particles shift position during etching, diminishing the regularity of the array. Continued RIE reduction completely destroys the NS's spherical shape (see Figure 1c).

The second critical issue relates to the formation of the metal layer with an array of holes by NS lift-off. When the NS diameter is reduced to a size comparable with the deposited metal film thickness, the metal layer deposited by the best line-of-sight deposition tool forms a continuous layer over the reduced spheres, making the lift-off process extremely challenging. Figure 1d shows incomplete lift-off of the PS NSs (≈120 nm in diameter) covered with a 25-nm-thick Au layer, even after extensive (>2 h) sonication in chloroform. Most of the PS NSs remain embedded in the metal film, resulting in little Si etching in the MACE solution and few, if any, NWs. Those that do form are highly non-uniform.

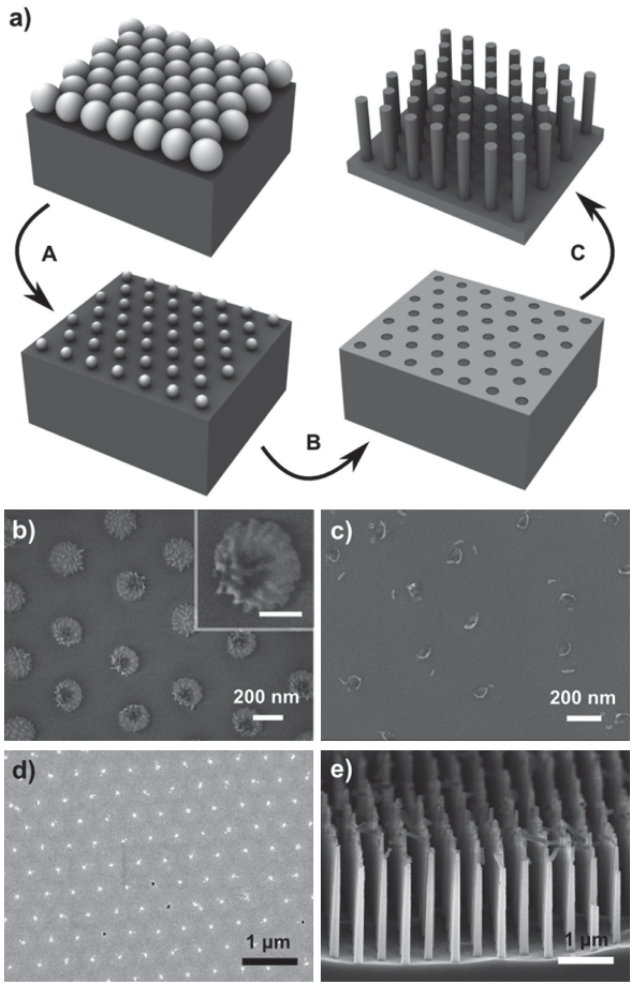

Figure 1. a) A schematic of SiNW fabrication using NSL and MACE with three key steps: A) NS reduction, B) lift-off of the metal catalyst layer, and C) MACE. Scanning electron microscopy (SEM) images demonstrate the process challenges of each step, b) roughened PS NSs with the disrupted hexagonal array after RIE etching, (the inset image showing an individual NS with scale bar in 100 nm), c) NSs virtually destroyed after excessive RIE, d) incomplete liftoff of a Au layer, e) NWs becoming tapered and porous when etched using MACE.

The last challenge is the tendency for porosity to develop in SiNWs prepared under some MACE conditions. A sparse NW array entails the high coverage of the metal layer on the surface, and such high catalyst coverage slows down the etch rate. The resulting SiNWs etched in HF/H_2O_2 solution are often tapered, and the extended exposure to HF renders the top portion of the SiNWs highly porous and structurally unstable (see Figure 1e). In the following, we present approaches to address these challenges and create a sparse, periodic array of VA-SiNWs in a step-by-step manner.

2.1. NS Reduction

An ideal process for reducing PS NS arrays preserves the NS spherical shape, surface smoothness, and hexagonal symmetry of the array throughout the reduction process. The surface roughness that emerges on arrayed PS NSs etched by RIE subsequently disturbs the NS spherical shape and array regularity. Several previous studies reported procedures to etch NSs while retaining their spherical shape, surface smoothness, and hexagonal symmetry. Tan et al. used a mixture of CF_4 and O_2 in a conventional parallel-plate (PP) RIE unit and found that a higher concentration of CF_4, in addition to O_2 plasma, smoothed the surface morphology of PS particles, compared to NSs etched with pure O_2 or a high O_2 content mixture.[35a,40] However, a high CF_4 concentration also etched the underlying Si substrate, which is undesirable for subsequent processes. Plettl et al. developed an isotropic etching process with pure O_2 in a commercial ICP-RIE system, and demonstrated that a slow (≈10 nm min^{-1}), isotropic etch rate offered much better control over the size and morphology of the NSs.[36] All of these previous studies, however, stopped short of demonstrating a large-scale (more than 70% of the original diameter) size reduction with the same dimensional and morphological control. Here, we used a commercial ICP-RIE system and a plasma discharge with a mixture of O_2 and CF_4 (but a higher concentration of O_2) to reduce the NS diameters by almost 90%.

Figure 2 compares the etching performance of PP-RIE and ICP-RIE. The PS NSs were reduced from the same starting diameter (≈490 nm), and the process parameters were tuned to yield similar etch rates (Figure 2a). The SEM images of the etched NSs at comparable sizes are shown in Figure 2b–g for each process at different total etching times. The NSs etched in ICP-RIE retained their spherical shape and surface smoothness, as well as hexagonal symmetry throughout the etching process. The NSs were reduced to 55 nm in diameter, or about an 89% reduction (data shown later). Such large-scale reduction with retention of the NS shape has, to our knowledge, not been reported before. The smooth reduction was accomplished without sacrificing etch rate. The 89% reduction took place in just 70 s, for an etch rate of 6.4 nm s^{-1}; about forty times faster than similar work.[36] By comparison, in PP-RIE, the NSs disintegrated when their diameter was reduced by more than 75% (similar to Figure 1c).

Three metrics were used to quantitatively assess the improvement in NS reduction by ICP-RIE compared to PP-RIE: roughness factor, aspect ratio, and interparticle distance. The roughness factor is defined as a ratio between the actual perimeter of the two-dimensional projection of the etched sphere and the perimeter of a fitted ellipse of the same two-dimensional projection. The roughness factor quantifies the ruggedness (or smoothness) of the NSs after etching. Aspect ratio is one of the shape descriptors, and is defined as the ratio of the major and minor axis of the fitted ellipse of the etched sphere. The disturbance of the array lattice was quantified by using the interparticle distance distribution between the etched array and original array. Interparticle distance is a center-to-center distance between two adjacent etched spheres. The magnitude of the error bar (i.e., standard deviation) of the interparticle distance distribution reflects how much each array was disturbed from the original hexagonal symmetry during etching. Any increase from "1" for roughness factor and aspect ratio means that the spheres get rougher or more non-spherical. The larger the error bar for the interparticle distance distribution, the less symmetric the array lattice becomes.

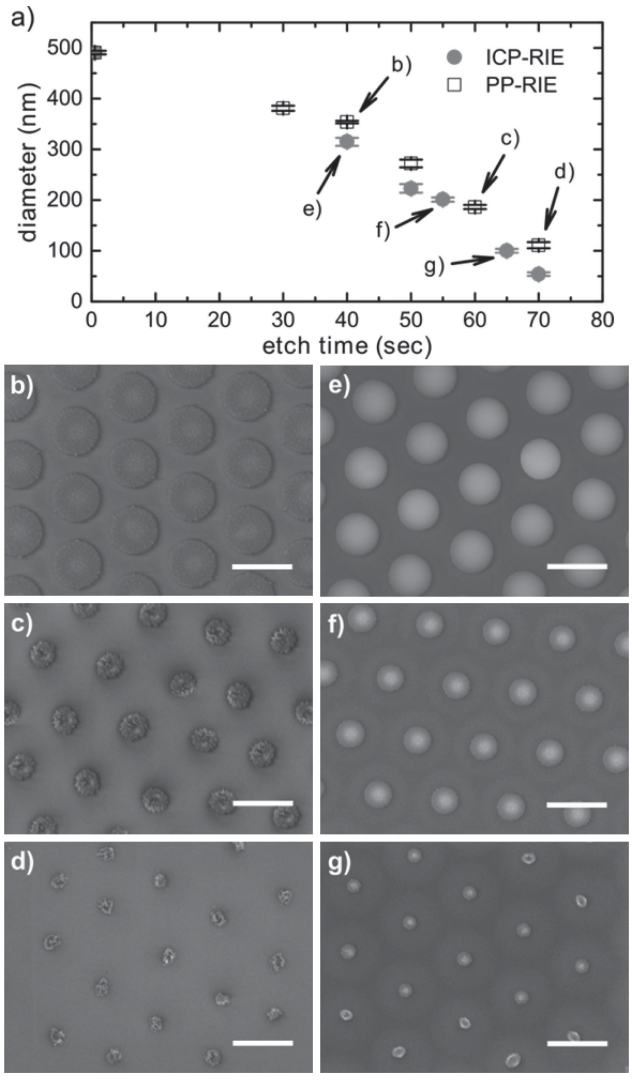

Figure 2. a) A plot of RIE etching time and reduced NS diameter in ICP-RIE and conventional PP-RIE; b–d) SEM images of an array of PS NSs that were etched for 40, 60, and 70 s, respectively, in PP-RIE; e–g) SEM images of an array of PS NSs that were etched for 40, 55, and 65 s, respectively, in ICP-RIE. (Scale bar is 400 nm.)

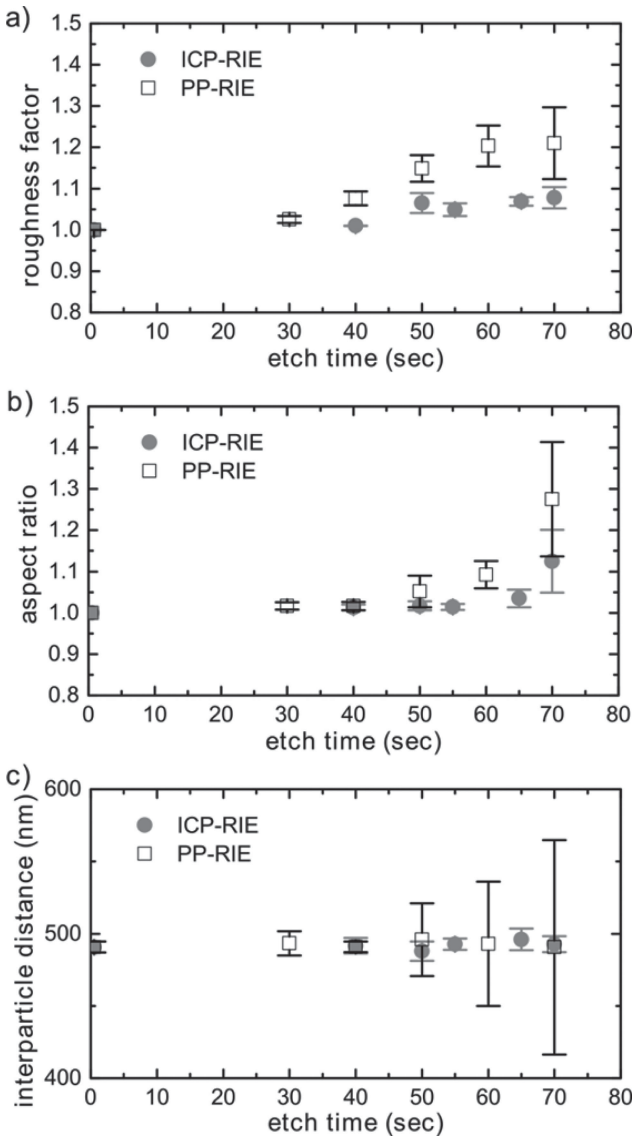

Figure 3. Plots of a) roughness factor, b) aspect ratio, and c) interparticle distance as a function of RIE etching time for ICP-RIE and PP-RIE. See the text for the definitions of roughness factor, aspect ratio, and interparticle distance. Error bars were constructed using standard errors (one standard deviation) based on the analysis of at least 15 NSs.

Figure 3 presents the roughness factor, aspect ratio, and interparticle distance distribution of NSs etched by the PP-RIE and ICP-RIE for different etch durations. Roughness factor values measured from PP-RIE-etched NSs were always higher than those from ICP-RIE-etched NSs, and the difference grew larger with increased etching. Before NS etching reached 50% size reduction, both PP-RIE and ICP-RIE produced similar aspect ratio and interparticle distance distribution values. After reduction by more than 50% (50 s or more etch time), the aspect ratio increased at a much faster rate for PP-RIE-etched NSs, meaning that reduced NSs became less and less spherical much more quickly. The error bar magnitude of interparticle distance distribution for the ICP-RIE-etched NSs was kept consistently small throughout the etching process. The interparticle distance distribution of the 89% reduced NSs was roughly the same as that of the original hexagonal close-pack array, indicating that the hexagonal array remained intact during the entire etching process.

Accurate control over the morphology, roughness, and hexagonal array can be attributed to a combination of the superior features of ICP-RIE and process optimization. In ICP-RIE, an ICP power (primarily responsible for generating plasma) and a platen power (used to adjust the dc bias) can be manipulated independently for better control of the plasma density and ion energy distribution.[41] Therefore, ICP-RIE enabled us to use a relatively high ICP power (e.g., 1000 W) for generating a large density of reactants while keeping the platen power low (≤10 W) to limit ion bombardment energy and anisotropic etching. In addition, including CF_4 in otherwise pure O_2 plasma greatly reduced the surface roughness during etching. With all other

parameters held constant, a plasma discharge consisting of 50% O_2 and 50% CF_4 resulted in NS etching almost twice as fast and yet significantly smoother than one with 100% O_2 (see Supporting Information, Figure S1). It has been proposed that, under a UV-ozone or oxygen plasma environment, low-molecular-weight backbone segments (e.g., C–C–C bonds) of PS cleave and convert to carboxyl functional groups.[42] The higher bond energy of these carboxyl functional groups means they persist longer in the oxygen plasma and therefore act as nanoscale masks for selective etching on PS NSs.[35b] We hypothesize that the addition of CF_4 to the discharge removes the carboxylate nanomasks that form on the NS surface, but additional study is needed for confirmation. The plasma discharge from a mixture of 20% CF_4 and 80% O_2 (40 sccm of O_2 and 10 sccm of CF_4) was ultimately selected as the best combination of smooth NS reduction and minimal substrate etching by excessive CF_4. Note, however, that a CF_4/O_2 discharge in PP-RIE did not produce as a smoother reduction as ICP-RIE (see Supporting Information, Figure S2). Other etching parameters, such as chamber pressure, gas flow rates, and mixture ratios, did not significantly alter the quality of NS reduction and were adjusted to optimize its etch rate.

Effective heat removal from the substrate was critical in preventing the spheres from disintegrating and in preserving the array's hexagonal symmetry. Plettl et al. reported that cryogenic temperature (around –150 °C) on the platen electrode helped to preserve the hexagonal symmetry of the array during etching.[36] In ICP-RIE, the substrate wafer is typically cooled with a flow of helium impinging onto the backside of the wafer. However, in many cases, the NSL substrate is much smaller than the platen electrode (here the sample is 2 cm × 2 cm while the platen is a 10 cm disk), so a carrier wafer of the same size as the platen is often used to cool the substrate during etching and facilitate the etching of small samples. However, it is difficult to remove energy (or heat) deposited into the sample during etching because of the high thermal resistance across the gap between the sample and carrier wafer. Application of vacuum thermal grease to the interface reduces the thermal contact resistance and helps cool the sample substrate, significantly improving the etch quality. The hexagonal symmetry of the array was well preserved at the platen temperature of 20 °C (i.e., no cryogenic temperature required), but etching at –20 °C produced the best results (Figure 2e–g).

2.2. Lift-off of the Metal Catalyst Layer

Reduced spheres are excellent lift-off masks because the re-entrant profile of the spherical shape breaks up the deposited film and thereby promotes solvent removal of the NSs during lift-off (see **Figure 4**a,e). For diameter of the reduced spheres ranging from 200 to <500 nm, the thickness of the Au catalyst layer was varied from 25 to 50 nm. The large ratio of the reduced sphere diameter to film thickness (>10) produced discontinuities in the metal layer and facilitated subsequent lift-off. Lift-off became increasingly difficult when the Au layer thickness exceeded a fifth of the sphere diameter. As shown in Figure 4b, an unbroken Au film limits the etchant access to the etching sites in the subsequent MACE process. This problem can be circumvented by depositing the Au film at an angle with respect to the substrate normal, creating a crescent shaped opening in the film on the shadowed side of the NS (see Figure 4c). Figure 4f shows a scanning electron microscopy (SEM) image of a 25-nm-thick Au film deposited at an incident angle of 30° onto NSs reduced to ≈50 nm in diameter. The resulting array of sub-10 nm openings in the film allows solvents to more easily reach the NSs for removal. An array of SiNWs etched from the film in Figure 4f is shown in Figure 4g. One distinct feature of this approach is that small, hinged Au cusps were created on the NSs during deposition and were not removed after lift-off or MACE. These cusps remained at the bases of the SiNWs (see the inset image of Figure 4g).

NS removal is also encouraged by reducing the metal film thickness so that the ratio of the Au thickness to the reduced sphere diameter is below roughly 0.2 (Figure 4d). However, the Au film can become discontinuous below a certain thickness, typically about 20 nm in an electron beam evaporator such as the one used here.[13b,43] Gold films below that thickness had irregular holes or were even discontinuous (see Figure 4h). MACE on such films resulted in extraneous ribbon-like features together with the SiNWs (see Figure 4i). This patchy Au film morphology is attributable to a low sticking coefficient, causing dewetting (Ostwald ripening) and delaying the growth of the continuous film.[44] We found that a thin layer (1–5 nm) of Ti served as an adequate adhesion layer for the Au film without affecting the Si etch rate during MACE. Figure 4j shows a 10-nm-thick Au film with a 1-nm-thick Ti adhesion layer. The film was continuous over the entire sample, as opposed to the Au film of the same thickness without the adhesion layer (Figure 4h).

Adding an adhesion layer before Au deposition not only decreases the critical thickness required for the continuous film, it also increases the robustness of the catalyst layer. The improved adhesion between the catalyst layer and the Si substrate prevents the film from delaminating during lift-off or MACE, thus improving the fabrication yield. The main concern in using an adhesion layer is whether it prevents intimate contact between the catalyst layer and the Si substrate, impeding catalytic etching. In order to investigate the effect of Ti on Si etching in an HF/H_2O_2 solution, four coupons were prepared with Ti thicknesses of 0 (straight Au), 1, 2, and 5 nm. We minimized other etching variables by fixing the metal surface area coverage (40%) as well as the Au thickness (25 nm). The samples were etched in a 5:1:1 solution of HF/H_2O_2/ethanol for different etching times. **Figure 5**a shows that the Si etch rate was not significantly affected by the different thicknesses of the Ti adhesion layer. In fact, the Au film without Ti exhibited the slowest etch rate. Three more samples of the same catalyst coverage (40%) and the same adhesion layer thickness (Ti = 1 nm) were prepared with different Au thickness (10, 15, and 25 nm). When etched in the same 5:1:1 solution of HF/H_2O_2/ethanol for different etching times, the overall etch rate was not significantly influenced by the Au thickness (Figure 5b). This experimental result corroborates the recent report that diffusion of etchants and byproducts along the Si/metal interface during MACE dominates diffusion through the metal film.[45] The NW length increased linearly with etching time for all cases, which agrees with previous studies.[13b,46]

Ti etches rapidly in an aqueous mixture of HF and H_2O_2 (>200 nm min^{-1}).[47] Therefore, the Ti adhesion layer may

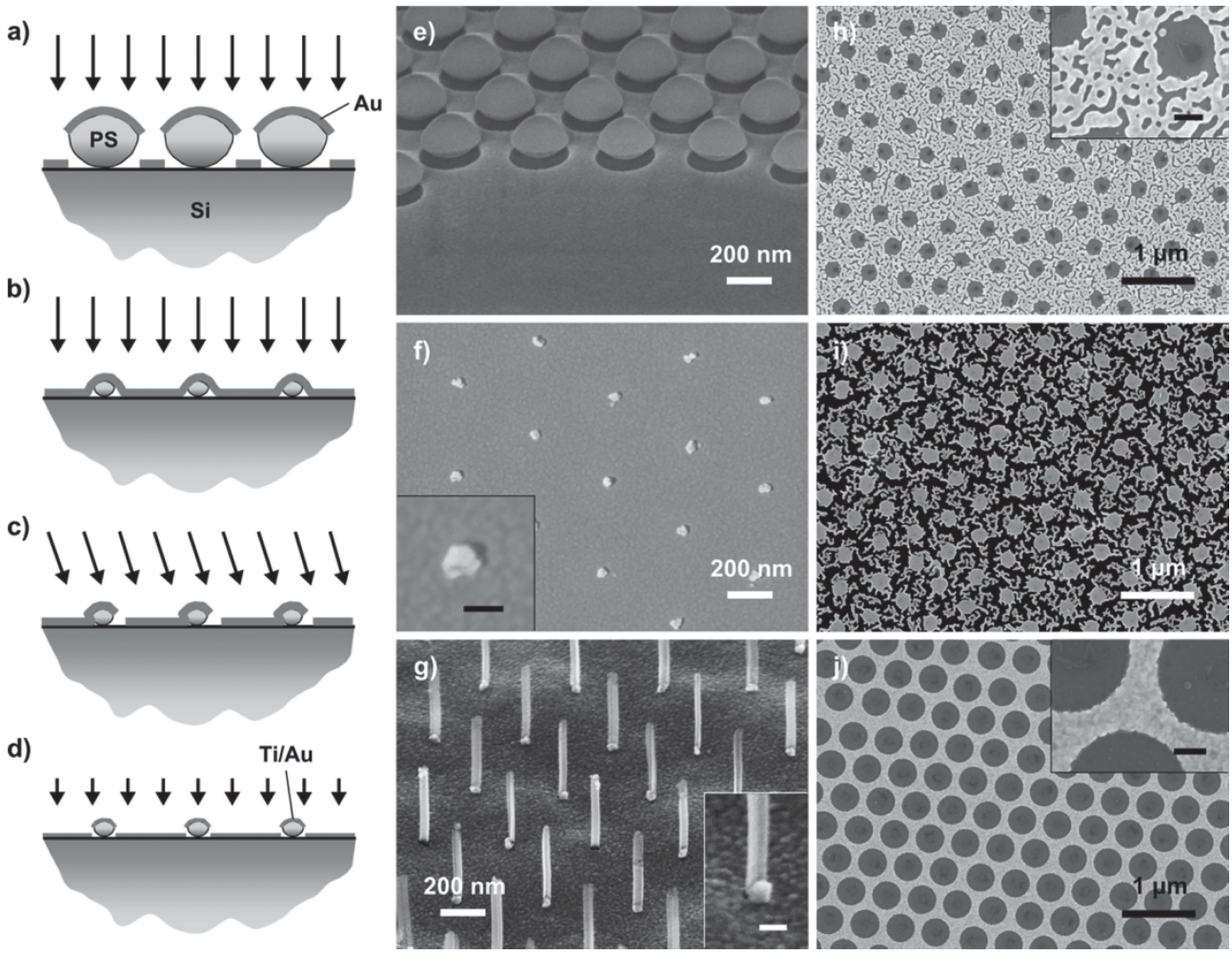

Figure 4. Schematics of metal deposition on reduced NS arrays showing a) a discontinuous Au film for NSs with modest RIE reduction, b) a continuous Au film deposited over NSs reduced by >80%, c) angled-deposition using shadowing by the reduced NSs to create openings in the Au film, and d) a thin (10 nm) Au film with a Ti adhesion layer deposited over reduced NSs. SEM images showing e) an array of reduced 280-nm NSs covered with 25 nm of Au deposited normal to the substrate, f) 52-nm NSs covered with 25 nm of Au deposited at 30° from normal, and g) an array of SiNWs etched from (f). SEM images showing the effect of the Ti adhesion layer; h) a 10-nm-thick Au film with no Ti after NS liftoff, i) top view of an array of SiNWs etched from (h) using MACE, and j) a 10-nm-thick Au film with a 1-nm-thick Ti adhesion layer after lift-off. Scale bars of inset images: 50 nm in (f,g) and 100 nm in (h,j).

dissolve almost instantly, bringing the Au layer into an intimate contact with the Si substrate, and allowing MACE of Si to occur regardless of the Ti adhesion layer thickness. Another common adhesion layer, Cr, is stable in the etchant solution, and so prevents contact between the Au and the Si substrate. No Si etching was reported with a Cr/Au layer because Cr itself does not act as a MACE catalyst.[45,48]

2.3. Metal-assisted Chemical Etching of a Sparse SiNW Array

Sparsely perforated gold layers deposited on NSs reduced by 70% or more have a high catalyst coverage (see Supporting Information, Figure S3, for the definition of catalyst coverage). As introduced in Figure 1e, MACE of Si using these sparsely perforated Au layers (i.e., catalyst coverage of over 90%) produces highly porous and tapered SiNWs. Similar to the previous report,[49] a gradually increasing density of nanopores and lateral etching (tapering) was observed from the root (bottom part) to the tip of the SiNWs. When etched in the same solution, a SiNW array with lower catalyst coverage (40–60%) was not porosified and did not taper at the tips (see Figure S4, Supporting Information). The pore formation mechanism may differ with the Si doping level and type,[27] but the SiNWs typically become more porous when i) the substrates are highly doped (<0.05 Ω cm),[16b,50] ii) the MACE etchant is H_2O_2 (or oxidant) rich,[8,11a] and iii) the less stable metal (e.g., Ag) is used as catalyst.[15,51] Here, a lightly doped N-type wafer (8–12 Ω cm) was used with stable Au as a catalyst and HF-rich etchant (ρ = [HF]/([HF] + [H_2O_2]) >0.9), all of which encourage the formation of non-porous SiNWs. The fact that we observed more porosification for SiNWs with high catalyst coverage under otherwise identical etching conditions suggests that the ratio of Si and Au areas exposed to the etchant affects the porosity of SiNWs. A possible explanation is

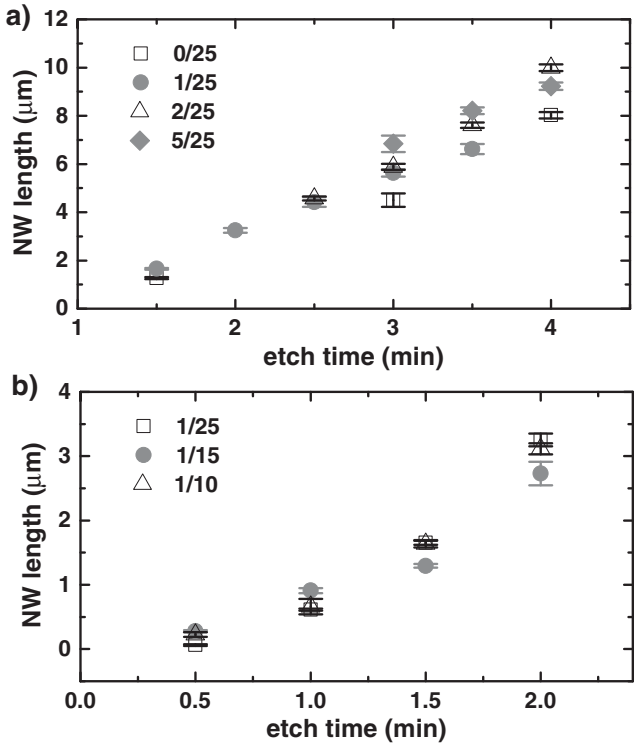

Figure 5. Plots of NW lengths vs etch time showing a) the effect of the Ti thickness on MACE for a fixed Au thickness and b) the effect of the Au thickness on MACE for a fixed Ti thickness. Note that p/q in each legend indicates the p-nm-thick Ti adhesion layer and the q-nm-thick Au layer. The areal coverage of catalyst was held constant at 40%.

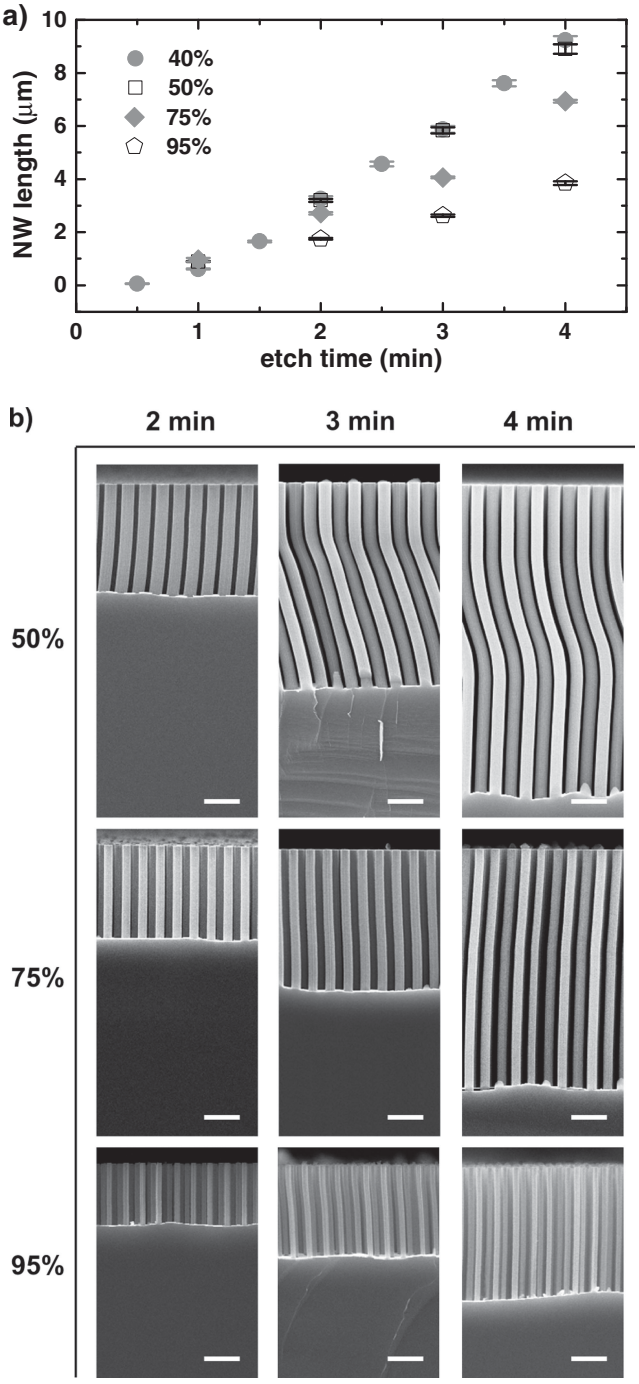

Figure 6. a) Plot of NW lengths vs etch times, showing the effect of the catalyst coverage on MACE. The catalyst layer was fixed at 1/25 nm (=Ti/Au). The same MACE solution ($HF:H_2O_2$:ethanol = 5:1:1) was used for all samples. b) SEM cross-sectional views of SiNW arrays with the same pitch (≈490 nm) and different diameters (370 nm for 50%, 260 nm for 75%, and 120 nm for 95%) etched for different times. (All scale bars represent 1 μm in length.)

that more holes are produced upon reduction of H_2O_2 due to the much larger available Au surface. The unconsumed/excessive holes injected into the Si diffuse to the SiNW sidewalls, causing porosification. In other words, MACE with high catalyst coverage creates an etching environment analogous to etching in a higher concentration of H_2O_2 (i.e., hole-rich environment). Moreover, the HF and H_2O_2 concentrations (for the same ρ) were important because etchants diluted in water etched more slowly and thus required longer etch times to achieve a given length of SiNWs. We found longer etch times increased the SiNW porosity, which is consistent with the others work.[49] The etching solution used in Figure S4, Supporting Information, was $HF:H_2O_2:H_2O$ = 10:1:40, and more concentrated etchant significantly decreased porosity and tapering (data shown below).

Catalyst coverage also affects the etch rate as shown in **Figure 6**a. Gold films with various hole diameters but the same pitch were prepared to yield catalyst coverage ranging from 40% to 99% (see Figure S3b, Supporting Information). As shown in Figure 6b, the etch rate of the sample with 50% metal coverage was more than twice as fast as that of the sample with 95% coverage. A decreasing etch rate with increasing catalyst coverage is consistent with a previous report,[46] but our experiments were conducted in large-area arrays and with a wider range of metal coverage. The reason for the slower etch rate on sparse SiNW arrays is two-fold. First, the local concentrations of oxidant (H_2O_2) and etchant (HF) are depleted more rapidly at high Au coverage because more Si area is subjected to the reaction, similar to loading effects in plasma etching.[52] Second, since the etchants access the metal/Si interface from the edge of the catalyst layer,[13b,45] they must travel farther along the metal/Si interface on sparse arrays. The combined effect substantially

decreases the etch rate, so more etching time is needed for the sparse SiNW array to achieve a given length of NWs. This extended contact with the etching solution allows uncatalyzed etching, which produces tapering and porosity. When a more concentrated etching solution was used (e.g., HF:H_2O_2:ethanol = 5:1:1), a sparse array of high aspect ratio SiNWs was obtained without noticeable tapering and porosification of the NW tips (see 95% and 4 min image in Figure 6b). Meanwhile, curved SiNWs were sometimes observed for the sample with low catalyst coverage (<70%, see 50% and 3 or 4 min image in Figure 6b). Switching the etching direction from the crystallographically preferred <100> planes to other orientations has been investigated by many researchers,[53] and a mechanism relevant to the present work may be the diffusion-controlled local variations of etchant concentrations near the etching front.[17]

Thus far, we have demonstrated methods for ultra-large-scale NS reduction, efficient metal lift-off and optimal MACE of a high-coverage metal layer, resulting in a sparse array of smooth SiNWs. This result demonstrates that these methods compare favorably to top-down patterning steps that involve slow and/or expensive equipment.[6,37] Our method retains the essential merits of NSL and MACE, that is, the rapid, inexpensive and scalable fabrication of sparse, yet high quality SiNW arrays. **Figure 7**a shows the SEM image of an array of etched

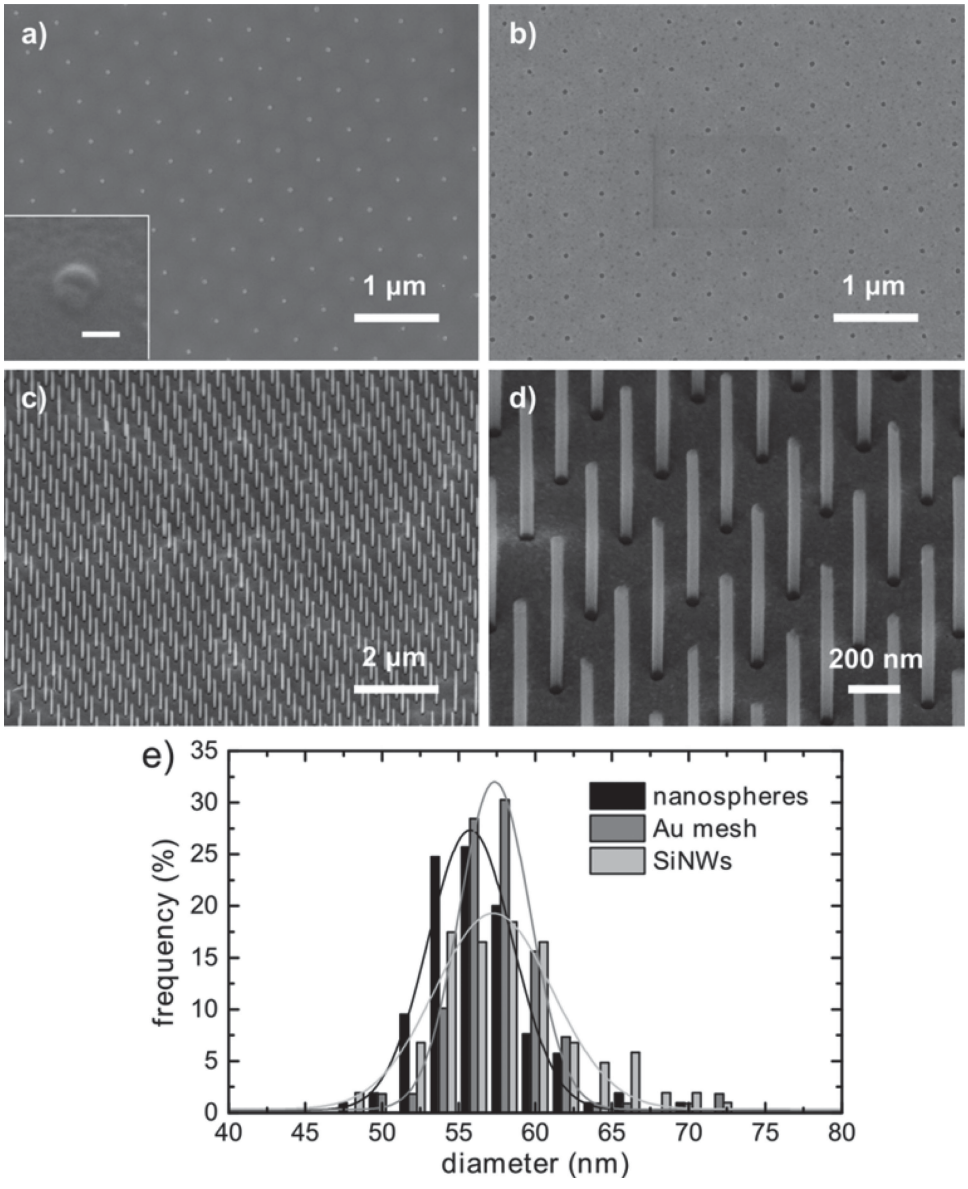

Figure 7. SEM images of a) PS NSs reduced from 490 to 55 nm by ICP-RIE (inset image: an individual reduced NS viewed from 45° (scale bar = 50 nm)), b) a 10-nm-thick Au layer with a 1-nm thick Ti adhesion layer after NS lift-off, c–d) an ordered and sparse array of SiNWs fabricated using the MACE process—the average wire diameter is 57 nm while the pitch (distance between two adjacent NWs) is maintained at 490 nm, e) size-distribution of 110 individual reduced NSs, nanoholes in the Au/Ti film, and SiNWs. From the Gaussian fit, the average diameter of the reduced NSs was 56 nm and the standard deviation was 4 nm. The average diameter and standard deviation of the nanoholes in the Au/Ti mesh were 57 nm and 4 nm, respectively, while those of the SiNWs were 57 nm and 5 nm.

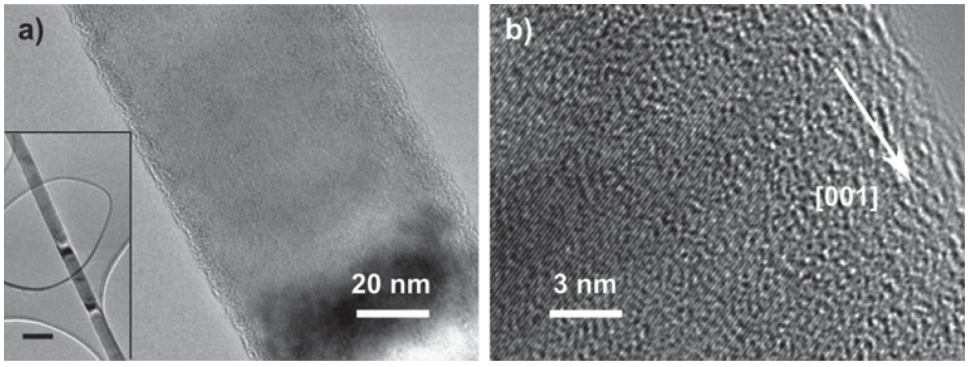

Figure 8. Transmission electron microcopy images of a solid SiNW (65 nm in diameter, 8–12 Ω cm n-Si, 10:1:2 of HF:H_2O_2:ethanol) with a) low magnification (the inset scale bar is 100 nm) and b) high magnification.

PS NSs reduced in diameter from 490 nm to 55 nm, or an 89% size reduction. The single etched NS in the inset image shows that they retained their near-spherical shape. The small amount of CF_4 (≈20%) present during ICP-RIE helped the Si substrate remain relatively unetched. The sparse array of non-hexagonal close-packed NSs was coated with a 1-nm-thick Ti adhesion layer and 10-nm-thick Au catalyst layer. The NSs were then easily removed with chloroform, producing a sparsely perforated, but continuous metal film. The Ti adhesion layer increased the continuity of the 10 nm Au film, and the use of the thinner metal layer improved the NS lift-off yield to >99% (see Figure 7b) from <5%, when 25-nm of gold was used. The use of highly concentrated etchant and oxidant with the relative concentration ratio (ρ) higher than the stoichiometric ratio (HF:H_2O_2 = 5:1)[15,48] minimized the formation of tapered and porous SiNWs. For instance, when the sparsely perforated Au film (Figure 7b) was etched in a 20:1:4 mixture (by vol) of HF:H_2O_2:ethanol,[54] an array of SiNWs was created without severe tapering or porosification. Figure 7c shows a large array of sparse SiNWs with a diameter-to-pitch ratio of close to 1:10 that was prepared by etching for 5 min. The high molar concentration of HF and H_2O_2 increased the etch rate, reducing the overall contact time of the NWs to the etching solution. As a result, the individual NWs seen in Figure 7d are straight and non-porous. The size of the as-etched SiNWs correlated strongly to the size of the reduced NSs and the perforated holes in the metal layer, as shown in the histogram of the SiNW diameters and the size of the spheres and nanoholes in Figure 7e. The Gaussian fit shows that the mean diameter and the standard deviation of the SiNWs (57 ± 5 nm) closely match with those of the etched NSs (56 ± 4 nm) and the nanoholes in the catalyst layer (57 ± 4 nm). A narrow size distribution also suggests that fine tuning of diameter and spacing of SiNW arrays is feasible using our methods.

Finally, SiNW porosity was qualitatively investigated by transmission electron microscopy (TEM). **Figure 8**a,b shows low magnification and high resolution TEM images of a SiNW that was harvested from a sparse NW array. The continuous lattice fringes seen in Figure 8b indicate the single-crystalline nature of the resulting NWs. These TEM images also manifest the absence of any apparent pores in the SiNW and support our claim that the optimized MACE process produced a sparse array of solid NWs.

3. Conclusions

We have formed ordered and sparse arrays of VA-SiNWs using combined NSL and MACE. A large pitch-to-diameter ratio requires the dramatic but smooth reduction of the templating NSs, which was achieved using an O_2/CF_4 discharge in ICP-RIE. Inclusion of CF_4 in the plasma and substrate cooling were important for such a uniform, isotropic reduction. Retention of the NSs' smoothness, spherical morphology, and hexagonal placement enabled patterning of a highly ordered, sparsely perforated Au catalyst layer and fabrication of NWs with smooth sidewalls and spherical cross-section. To promote the lift-off of the Au layer atop reduced NSs, discontinuities in the metal film were intentionally introduced either by depositing at an off-normal incident angle or by decreasing the film thickness. The Ti adhesion layer played a pivotal role in enabling formation of thinner, defect-free Au films. The Ti was removed quickly by the MACE solution, thus bringing the Au film into intimate contact with the Si substrate. High molar concentration, HF-rich etchant mixtures decreased the formation of tapering and porosity in the tips of the SiNWs. The combination of all of these improved methods enabled a scalable and inexpensive fabrication of large-area, ordered and sparse VA-SiNW arrays. Such arrays are potentially useful in electronic/optical applications such as photonic crystals, vertical transistors, and biological applications, such as multifunctional platforms for guiding cell growth and functions.

4. Experimental Section

Substrate Preparation: Four-inch single-side polished silicon wafers (Montco Silicon, <100> orientation and 500 μm in thickness, N-type, 8–12 Ω cm) were cut into 2 cm by 2 cm coupons, which were ultrasonically cleaned in acetone and isopropyl alcohol. The Si coupons were further cleaned in piranha solution (3 parts of H_2SO_4 and 1 part of H_2O_2) for 30 min and subsequently in SC-1 solution (1 part of H_2O_2, 1 part of NH_4OH and 5 parts of deionized water) for 30 min to render their surfaces hydrophilic. The coupons were then thoroughly rinsed with DI water and stored in DI water until used.

Nanosphere Lithography: Colloidal monodispersed PS NSs with nominal diameters of 490 nm were purchased from Polysciences Inc. and mixed with a 400:1 solution of methanol:Triton X-100. In order to form a hexagonal close-pack monolayer, the NS solution was spin-coated onto each substrate at 400, 500, and 1400 rpm for 30 s, 2 min, and 10 s, respectively. Once completely dried, the NSs were etched in

an ICP-RIE (Oxford Plasmalab System 100) with a mixture of O_2 and CF_4 (0 to 50 sccm) at various ICP (300 to 2500 W) and RF power (3 to 20 W) levels and chamber pressures (12 to 40 mTorr). For comparison, a conventional parallel-plate (PP)-RIE system (March CS 1701) was also used to reduce the NS diameter. The PP-RIE etching parameters were 25 sccm of O_2, 150 W of RF power, and 320 mTorr of chamber pressure. The etching time was varied to yield the desired diameter reduction, leading to a hexagonal non-close-packed NS array. A gold nanomesh template for MACE was then generated by evaporating Au on the Si topped with the NS array (Temescal e-beam evaporator, background pressure less than 1×10^{-6} Torr). After the gold was evaporated, the NSs were removed by dissolution in $CHCl_3$ (Sigma-Aldrich). In most cases, mild sonication was used to accelerate lift-off. The Au thickness was changed from 10 to 25 nm, with and without a thin layer of Ti (1 to 5 nm) as an adhesion layer.

Silicon Nanowire Fabrication: The SiNWs were formed when the coupon was immersed into an etching mixture consisting of HF (49%), H_2O_2 (30%), and ethanol (DI water) as a diluent. The HF and H_2O_2 concentrations were varied to investigate the effect of etching mixtures on NW porosity. In a typical run, 150 mL of HF, 30 mL of H_2O_2 and 30 mL of ethanol (5:1:1 of HF:H_2O_2:ethanol) were mixed with a Teflon-coated stir bar. A mixture of 20:1:4 of HF:H_2O_2:ethanol was used to minimize porosity while etching sparse arrays of SiNWs.[54] The NW lengths were adjusted by changing the etching duration, which ranged from 30 s to 30 min. The remaining Au layer was removed in a gold etchant TFA (Transene). After rinsing the SiNW coupons in isopropanol alcohol multiple times, the coupons were dried under a stream of N_2. For long NWs, a CO_2 critical point dryer (Tousimis, Automegasamdri-815B) was used to prevent NWs from bundling.

Imaging and Analysis: SEM images were obtained using a Carl Zeiss SMT Supra 55 (field-emission high-resolution SEM) instrument. The SiNW lengths were measured from the SEM images of the cleaved SiNW samples. Image analysis was performed using the freeware software, ImageJ. TEM images were obtained using a JEOL 2010F electron microscope. SiNWs (average diameter = 65 ± 4 nm) etched with a concentrated MACE solution (10:1:2 of HF:H_2O_2:ethanol) were scratched off from a sparse NW array of the n-type substrate (8–12 Ω cm) and transferred to isopropanol alcohol. SiNWs were then dispersed in isopropanol alcohol with 20 min of sonication. A couple of drops of this mixture were applied to a lacey carbon film on a Cu TEM grid for imaging and analysis.

Supporting Information

Supporting Information is available from the Wiley Online Library or from the author.

Received: March 28, 2013
Revised: May 31, 2013
Published online: July 24, 2013

[1] V. Schmidt, J. V. Wittemann, S. Senz, U. Gösele, *Adv. Mater.* **2009**, *21*, 2681.
[2] a) Y. Cui, C. M. Lieber, *Science* **2001**, *291*, 851; b) S. Hoffmann, J. Bauer, C. Ronning, T. Stelzner, J. Michler, C. Ballif, V. Sivakov, S. H. Christiansen, *Nano Lett.* **2009**, *9*, 1341; c) Y. Cui, Z. Zhong, D. Wang, W. U. Wang, C. M. Lieber, *Nano Lett.* **2003**, *3*, 149.
[3] a) B. Tian, X. Zheng, T. J. Kempa, Y. Fang, N. Yu, G. Yu, J. Huang, C. M. Lieber, *Nature* **2007**, *449*, 885; b) V. Sivakov, G. Andra, A. Gawlik, A. Berger, J. Plentz, F. Falk, S. H. Christiansen, *Nano Lett.* **2009**, *9*, 1549.
[4] a) Y. Cui, Q. Wei, H. Park, C. M. Lieber, *Science* **2001**, *293*, 1289; b) J. Hahm, C. M. Lieber, *Nano Lett.* **2004**, *4*, 51.
[5] a) M. Shao, D. D. D. Ma, S.-T. Lee, *Eur. J. Inorg. Chem.* **2010**, *2010*, 4264; b) S. Barth, F. Hernandez-Ramirez, J. D. Holmes, A. Romano-Rodriguez, *Prog. Mater. Sci.* **2010**, *55*, 563.
[6] R. G. Hobbs, N. Petkov, J. D. Holmes, *Chem. Mater.* **2012**, *24*, 1975.
[7] a) T. Bryllert, L.-E. Wernersson, L. E. Fröberg, L. Samuelson, *IEEE Electron Device Lett.* **2006**, *27*, 323; b) J. Goldberger, A. I. Hochbaum, R. Fan, P. Yang, *Nano Lett.* **2006**, *6*, 973; c) V. Schmidt, H. Riel, S. Senz, S. Karg, W. Riess, U. Gösele, *Small* **2006**, *2*, 85.
[8] Y. Qu, L. Liao, Y. Li, H. Zhang, Y. Huang, X. Duan, *Nano Lett.* **2009**, *9*, 4539.
[9] S. M. Wells, I. A. Merkulov, I. I. Kravchenko, N. V. Lavrik, M. J. Sepaniak, *ACS Nano* **2012**, *6*, 2948.
[10] a) Z. Huang, H. Fang, J. Zhu, *Adv. Mater.* **2007**, *19*, 744; b) D. H. Lee, Y. Kim, G. S. Doerk, I. Laboriante, R. Maboudian, *J. Mater. Chem.* **2011**, *21*, 10359.
[11] a) C. Chartier, S. Bastide, C. Levy-Clement, *Electrochim. Acta* **2008**, *53*, 5509; b) M.-L. Zhang, K.-Q. Peng, X. Fan, J.-S. Jie, R.-Q. Zhang, S.-T. Lee, N.-B. Wong, *J. Phys. Chem. C* **2008**, *112*, 4444.
[12] O. J. Hildreth, W. Lin, C. P. Wong, *ACS Nano* **2009**, *3*, 4033.
[13] a) O. J. Hildreth, D. Brown, C. P. Wong, *Adv. Funct. Mater.* **2011**, *21*, 3119; b) Z. Huang, N. Geyer, P. Werner, J. de Boor, U. Goesele, *Adv. Mater.* **2011**, *23*, 285.
[14] K. Peng, A. Lu, R. Zhang, S.-T. Lee, *Adv. Funct. Mater.* **2008**, *18*, 3026.
[15] J. Kim, H. Han, Y. H. Kim, S.-H. Choi, J.-C. Kim, W. Lee, *ACS Nano* **2011**, *5*, 3222.
[16] a) A. I. Hochbaum, R. Chen, R. D. Delgado, W. Liang, E. C. Garnett, M. Najarian, A. Majumdar, P. Yang, *Nature* **2008**, *451*, 163; b) A. I. Hochbaum, D. Gargas, Y. J. Hwang, P. Yang, *Nano Lett.* **2009**, *9*, 3550.
[17] J. Kim, Y. H. Kim, S.-H. Choi, W. Lee, *ACS Nano* **2011**, *5*, 5242.
[18] a) K. Q. Peng, Y. Xu, Y. Wu, Y. J. Yan, S. T. Lee, J. Zhu, *Small* **2005**, *1*, 1062; b) Y. Li, J. Zhang, S. Zhu, H. Dong, Z. Wang, Z. Sun, J. Guo, B. Yang, *J. Mater. Chem.* **2009**, *19*, 1806; c) T.-H. Pei, S. Thiyagu, Z. Pei, *Appl. Phys. Lett.* **2011**, *99*, 153108.
[19] a) M. K. Dawood, H. Zheng, T. H. Liew, K. C. Leong, Y. L. Foo, R. Rajagopalan, S. A. Khan, W. K. Choi, *Langmuir* **2011**, *27*, 4126; b) Y. Chen, Z. G. Guo, J. S. Xu, L. Shi, J. Li, Y. B. Zhang, *MRS Bull.* **2012**, *47*, 1687.
[20] F.-Y. Wang, Q.-D. Yang, G. Xu, N.-Y. Lei, Y. K. Tsang, N.-B. W. J. C. Ho, *Nanoscale* **2011**, *3*, 3269.
[21] a) C. K. Chan, H. L. Peng, G. Liu, K. McIlwrath, X. F. Zhang, R. A. Huggins, Y. Cui, *Nat. Nanotechnol.* **2008**, *3*, 31; b) R. Huang, X. Fan, W. Shen, J. Zhu, *Appl. Phys. Lett.* **2009**, *95*, 133119.
[22] a) B. H. Zhang, H. S. Wang, L. H. Lu, K. L. Ai, G. Zhang, X. L. Cheng, *Adv. Funct. Mater.* **2008**, *18*, 2348; b) K. Q. Peng, X. Wang, S. T. Lee, *Appl. Phys. Lett.* **2009**, *95*, 143119; c) H. J. In, C. R. Field, P. E. Pehrsson, *Nanotechnology* **2011**, *22*, 355501.
[23] B. M. Kayes, H. A. Atwater, N. S. Lewis, *J. Appl. Phys.* **2005**, *97*, 114302.
[24] K. Seo, M. Wober, P. Steinvurzel, E. Schonbrun, Y. P. Dan, T. Ellenbogen, K. B. Crozier, *Nano Lett.* **2011**, *11*, 1851.
[25] J. M. Weisse, C. H. Lee, D. R. Kim, X. L. Zheng, *Nano Lett.* **2012**, *12*, 3339.
[26] a) W. K. Choi, T. H. Liew, M. K. Dawood, H. I. Smith, C. V. Thompson, M. H. Hong, *Nano Lett.* **2008**, *8*, 3799; b) M. K. Dawood, T. H. Liew, P. L. M. H. Hong, S. Tripathy, J. T. L. Thong, W. K. Choi, *Nanotechnology* **2010**, *21*, 205305.
[27] B. Mikhael, B. Elise, M. Xavier, S. Sebastian, M. Johann, P. Laetitia, *ACS Appl. Mater. Interfaces* **2011**, *3*, 3866.
[28] B. M. Bang, H. Kim, J.-P. Lee, J. Cho, S. Park, *Energy Environ. Sci.* **2011**, *4*, 3395.
[29] J. Huang, S. Y. Chiam, H. H. Tan, S. Wang, W. K. Chim, *Chem. Mater.* **2010**, *22*, 4111.

[30] O. J. Cayre, V. N. Paunov, *J. Mater. Chem.* **2004**, *14*, 3300.
[31] P. Jiang, M. J. McFarland, *J. Am. Chem. Soc.* **2005**, *127*, 3710.
[32] X. Yan, J. M. Yao, G. Lu, X. Li, J. H. Zhang, K. Han, B. Yang, *J. Am. Chem. Soc.* **2005**, *127*, 7688.
[33] Y. Li, E. J. Lee, W. Cai, K. Y. Kim, S. O. Cho, *ACS Nano* **2008**, *2*, 1108.
[34] C. Haginoya, M. Ishibashi, K. Koike, *Appl. Phys. Lett.* **1997**, *71*, 2934.
[35] a) B. J. Y. Tan, C. H. Sow, K. Y. Lim, F. C. Cheong, G. L. Chong, A. T. S. Wee, C. K. Ong, *J. Phys. Chem. B* **2004**, *108*, 18575; b) H. Y. Hsieh, J. L. Xiao, C. H. Lee, T. W. Huang, C. S. Yang, P. C. Wang, F. G. Tseng, *J. Phys. Chem. C* **2011**, *115*, 16258.
[36] A. Plettl, F. Enderle, M. Saitner, A. Manzke, C. Pfahler, S. Wiedemann, P. Ziemann, *Adv. Funct. Mater.* **2009**, *19*, 3279.
[37] M. Khorasaninejad, N. Abedzadeh, A. S. Jawanda, O. Nixon, M. P. Anantram, S. S. Saini, *J. Appl. Phys.* **2012**, *111*, 044328.
[38] M. Khorasaninejad, N. Abedzadeh, J. Walia, S. Patchett, S. S. Saini, *Nano Lett.* **2012**, *12*, 4228.
[39] M. A. Bucaro, Y. Vasquez, B. D. Hatton, J. Aizenberg, *ACS Nano* **2012**, *6*, 6222.
[40] B. J. Y. Tan, C. H. Sow, T. S. Koh, K. C. Chin, A. T. S. Wee, C. K. Ong, *J. Phys. Chem. B* **2005**, *109*, 11100.
[41] J. Yeom, Y. Wu, J. C. Selby, M. A. Shannon, *J. Vac. Sci. Technol. B* **2005**, *23*, 2319.
[42] a) S. Guruvenket, G. M. Rao, M. Komath, A. M. Raichur, *Appl. Surf. Sci.* **2004**, *236*, 278; b) A. Mahfoudh, J. Barbeau, M. Moisan, A. Leduc, J. Seguin, *Appl. Surf. Sci.* **2010**, *256*, 3063.
[43] X. Li, P. W. Bohn, *Appl. Phys. Lett.* **2000**, *77*, 2572.
[44] a) C. M. Mueller, F. C. F. Mornaghini, R. Spolenak, *Nanotechnology* **2008**, *19*, 485306; b) H. Sun, M. Yu, G. Wang, X. Sun, J. Lian, *J. Phys. Chem. C* **2012**, *116*, 9000.
[45] N. Geyer, B. Fuhrmann, Z. Huang, J. de Boor, H. S. Leipner, P. Werner, *J. Phys. Chem. C* **2012**, *116*, 13446.
[46] K. Rykaczewski, O. J. Hildreth, C. P. Wong, A. G. Fedorov, J. H. J. Scott, *Nano Lett.* **2011**, *11*, 2369.
[47] K. R. Williams, R. S. Muller, *J. Microelectromech. Syst.* **1996**, *5*, 256.
[48] W. Chern, K. Hsu, I. S. Chun, B. P. de Azeredo, N. Ahmed, K.-H. Kim, J.-M. Zuo, N. Fang, P. Ferreira, X. Li, *Nano Lett.* **2010**, *10*, 1582.
[49] G. D. Yuan, R. Mitdank, A. Mogilatenko, S. F. Fischer, *J. Phys. Chem. C* **2012**, *116*, 13767–.
[50] Y. Qu, H. Zhou, X. Duan, *Nanoscale* **2011**, *3*, 4060.
[51] K. Tsujino, M. Matsumura, *Adv. Mater.* **2005**, *17*, 1045.
[52] C. J. Mogab, *J. Electrochem. Soc.* **1977**, *124*, 1262.
[53] a) C.-Y. Chen, C.-S. Wu, C.-J. Chou, T.-J. Yen, *Adv. Mater.* **2008**, *20*, 3811; b) Z. Huang, T. Shimizu, S. Senz, Z. Zhang, X. Zhang, W. Lee, N. Geyer, U. Gösele, *Nano Lett.* **2009**, *9*, 2519; c) H. Chen, H. Wang, X.-H. Zhang, C.-S. Lee, S.-T. Lee, *Nano Lett.* **2010**, *10*, 864; d) Z. Huang, T. Shimizu, S. Senz, Z. Zhang, N. Geyer, U. Goesele, *J. Phys. Chem. C* **2010**, *114*, 10683.
[54] K. Balasundaram, J. S. Sadhu, J. C. Shin, B. Azeredo, D. Chanda, M. Malik, K. Hsu, J. A. Rogers, P. Ferreira, S. Sinha, X. L. Li, *Nanotechnology* **2012**, *23*, 305304.